

RESEARCH

Open Access



Dynamic transcriptome and metabolome analyses of two sweet corn lines under artificial aging treatment

Zili Zhang¹, Ruichun Yang², Lei Gao³, Shilin Huang², Feng Jiang¹, Qingchun Chen¹, Pengfei Liu^{1*} and Faqiang Feng^{2*}

Abstract

Background Strong tolerance to seed aging is an important agricultural trait for sweet corn production. Previous studies have primarily focused on the QTLs for the seed vigor. However, there were few researches involving in the metabolome and transcriptome of artificial aging seeds.

Results Using two inbred lines with significant differences in seed artificial aging tolerance, RNA sequencing and non-targeted metabolomic analysis were employed to extensively evaluate transcripts and metabolites in seeds that underwent artificial aging. Fourteen common transcripts and 16 common metabolites with sustained differential expression were identified in the two lines, suggesting their potential necessity in seed response to artificial aging. Enrichment analysis of differentially expressed genes (DEGs) in the transcriptome at different stages revealed significant enrichment KEGG pathways, "Oxidative phosphorylation" was the common pathway in the 0d vs 3d comparison for K107 and L155. The identical enriched KEGG pathways were observed in the 3d vs 6d comparison for K107 and 0d vs 6d comparison for L155, indicating a slower transcriptomic response in the aging-tolerance line. DEGs at 0 days between the two lines had been enriched in the "Terpenoid backbone biosynthesis" and "Ribosome" pathways, while at 6 days, the enrichment pathway were "Sulfur metabolism", "Linoleic acid metabolism", and "Plant hormone signal transduction". A total of 312 differentially expressed metabolites (DEMs) were found at 0, 3 and 6 days after seed aging treatment, and they shared enriched metabolic pathway of "ABC transporters". The KEGG enrichment of DEGs and DEMs shared the common pathway, namely "Linoleic acid metabolism". Among these, the most abundant metabolites were Glutathione, Adenosine, Trehalose, and 10E,12Z-Octadecadienoic acid. Focusing on the ascorbate–glutathione pathway revealed that the difference in ROS production and the ROS scavenging capability mediated by *glutathione S-transferase (GST)* genes were important factors contributing to the differing seed aging tolerance in the two lines.

Conclusion In summary, these results contribute to a deeper understanding of the overall mechanisms underlying artificial aging tolerance in sweet corn seeds. The findings of this study are expected to provide valuable insights for the storage of sweet corn seeds.

Keywords Sweet corn, Artificial aging, Transcriptome, Metabolome

*Correspondence:

Pengfei Liu

774990480@qq.com

Faqiang Feng

fengfq@scau.edu.cn

Full list of author information is available at the end of the article



© The Author(s) 2025. **Open Access** This article is licensed under a Creative Commons Attribution-NonCommercial-NoDerivatives 4.0 International License, which permits any non-commercial use, sharing, distribution and reproduction in any medium or format, as long as you give appropriate credit to the original author(s) and the source, provide a link to the Creative Commons licence, and indicate if you modified the licensed material. You do not have permission under this licence to share adapted material derived from this article or parts of it. The images or other third party material in this article are included in the article's Creative Commons licence, unless indicated otherwise in a credit line to the material. If material is not included in the article's Creative Commons licence and your intended use is not permitted by statutory regulation or exceeds the permitted use, you will need to obtain permission directly from the copyright holder. To view a copy of this licence, visit <http://creativecommons.org/licenses/by-nc-nd/4.0/>.

Background

Sweet corn (*Zea mays* L. *Saccharata* Sturt), derived from the mutations of one or a few relative genes regulating the conversion of sugar to starch within the endosperm, exhibits a delightful flavor and high sugar content, making it a popular choice for cultivation worldwide [1, 2]. However, its mature seeds possess low starch content, resulting in shrunken seeds with poor storage tolerance, consequently impacting seed germination and seedling vigor [3]. Notably, South China was the primary production region for sweet corn in China [4], where sweet corn seeds for field production are sown in autumn and subsequently introduced to the market in the following spring, entailing a storage period of approximately 4–6 months. The humid and rainy climate characteristic of South China accelerates the aging and deterioration of seeds, significantly impairing their storage capacity and thereby influencing the production of sweet corn. Given the crucial role of high-quality seeds in sweet corn production, further exploration of genetic and metabolic mechanisms governing tolerance to aging becomes an imperative goal in sweet corn breeding.

Seed aging is a complex process characterized by irreversible decline in seed vigor during storage. Seed aging and deterioration involves irreversible metabolic and cellular changes, like reduced antioxidant capacity, cell membrane disruption, genetic material damage, protein degradation, and decreased energy metabolism [5]. Highly reactive and toxic ROS can damage cell membranes, nucleic acids, proteins, carbohydrates, and lipids, causing irreversible cell system damage [6]. During seed deterioration, ROS accumulate, including singlet oxygens ($^1\text{O}_2$), superoxide radicals ($\text{O}_2^{\cdot-}$), hydrogen peroxide (H_2O_2), and hydroxyl radicals (OH^{\cdot}) [7]. Thus, lipid peroxidation and cell membrane disruption caused by free radicals are major damages in the aging process [8]. Seeds contain many antioxidant enzymes to protect against excessive ROS. Key ones are superoxide dismutase (SOD), catalase (CAT), ascorbate peroxidase (APX), etc. [5]. The ascorbate—glutathione cycle is crucial in response to seed aging [9, 10]. The weakening of the antioxidant system, especially reduced enzymatic activities, may lead to the loss of seed vigor [9].

Seed deterioration is an inevitable process, influenced by both genetic and environmental factors, even in optimal conditions. To date, maize seed aging research has predominantly centered on physiological alterations [3, 11] and QTL mapping. Under different artificial aging conditions, 65 QTLs for four seed vigor traits and 18 meta-QTLs were detected by Han et al. [12]. Ku et al. [13] identified 74 QTLs and 20 trait-related mQTLs for the mean germination time and other related seed vigor traits. In the recombinant inbred line (RIL) and IF₂

populations, Wang et al. [14] found 49 QTLs for four measured seed vigor traits. From two connected RIL populations, Han et al. [15] detected 74 QTLs and 20 mQTLs for seed vigor. Employing an F_{2,3} population and a RIL population, 13 QTLs were identified to be located on five chromosome regions for seed artificial aging [16]. Currently, there have been no published reports regarding the map-based cloning of seed vigor genes in maize.

The expansion of high-quality sequence data and the generation of large-scale omics datasets have effectively enhanced the comprehensive understanding of the intricate process of seed aging. Transcriptome investigations on seed aging have been carried out in multiple plant species such as pea [17], soybean [18], maize [19], oat [20], and rice [21]. For example, research has identified key genes associated with oxidative stress and programmed cell death during the aging of pea seeds [17]. Comparative analysis of the transcriptomes of aged and fresh soybean seeds has revealed that the time-dependent relationship between transcript fragmentation and length can be a useful indicator of age-related damage [18]. In maize, by comparing the transcriptome profiles of two chromosome segment substitution lines with accelerated-aged seeds, 13 DEGs were detected within the mapping interval [19]. Through transcriptomic analysis of oat embryos during seed aging, changes in energy production and the AsA-GSH cycle were elucidated [10]. In rice, specific long-lived mRNAs related to seed longevity were identified [20]. Moreover, the dysfunction of antioxidant and glyoxalase system, and the accumulation of ROS and methylglyoxal definitely contribute to seed aging, and a putative model for aging response and self-detoxification mechanisms was proposed based on full-length transcriptome in oat [21].

Metabolites, the end products of cellular processes, serve as the final manifestations of biological systems' responses to genetic or environmental changes. Despite their significance, the metabolome of aging plant seeds has received relatively little research attention. In maize, it has been discovered that *ZmDREB2 A* regulates the longevity of maize seeds. This occurs by promoting the production of raffinose, which in turn regulates *ZmGH3.2* and *ZmRAFS*, thereby redirecting metabolism to enhance seed aging tolerance [22]. Additionally, it has been reported that the maize alkaline α -galactosidase 1 protein is translationally induced and can hydrolyze raffinose family oligosaccharides (RFOs). Overexpression of *ZmAGA1* in *Arabidopsis* has been shown to reduce seed aging tolerance in mature dry seeds [23]. Regarding soybean (*Glycine max* L. Merr.), dynamic changes in membrane lipid metabolism and antioxidant defense during seed aging have been detected [8].

Sweet corn seeds typically possess low vigor, and their poor storage tolerance substantially impacts production and marketability. A review of omics research on seed aging reveals that most studies have concentrated on transcriptome and proteome analysis, while metabolomics has received relatively less attention. In this study, two sweet corn inbred lines with marked differences in seed-aging tolerance were selected for investigation. K107 was determined to be the seed-aging-sensitive line [24]. L155, derived from the RIL population of K107 and K62, exhibited greater tolerance to seed aging compared to K62 [25]. Seed samples were collected 0, 3, and 6 days after artificial accelerated aging. RNA sequencing and widely-targeted metabolomics techniques were employed to comprehensively analyze transcripts and metabolites, respectively. This methodology aimed to elucidate the differences in transcripts and metabolites between the two lines after seed aging. The main objective of this study is to elucidate the regulatory mechanisms that contribute to sweet corn's tolerance against seed aging, thereby offering theoretical insights to support the advancement of long-term preservation techniques for sweet corn seeds.

Results

Morphological characteristics of seeds after aging

As depicted in Fig. 1, it is evident that with an increase in the duration of artificial aging treatment, four seed vigor indicators for both lines showed a declining trend. Post artificial aging treatment, four seed vigor indicators of L155 were significantly higher than those of K107. Initially, at 0 days after artificial aging treatment, the differences in germination potential (GP) and germination rate (GR) between L155 and K107 did not reach the significant level of 0.05; however, the germination index (GI) and vigor index (VI) of L155 were significantly higher than those of K107. After 3 and 6 days of artificial aging treatment, L155 exhibited significantly higher values across four seed vigor indicators compared to K107.

Evaluation of mRNA sequencing data

To comprehensively elucidate the transcriptional and metabolic alterations occurring in sweet corn seeds during artificial aging, an extensive analysis was conducted employing widely targeted metabolomics and RNA-Seq on seeds subjected to artificial aging at 0, 3, and 6 days. For RNA-Seq, each time point comprised 3 independent replicates, resulting in a total of 18 sequenced libraries.

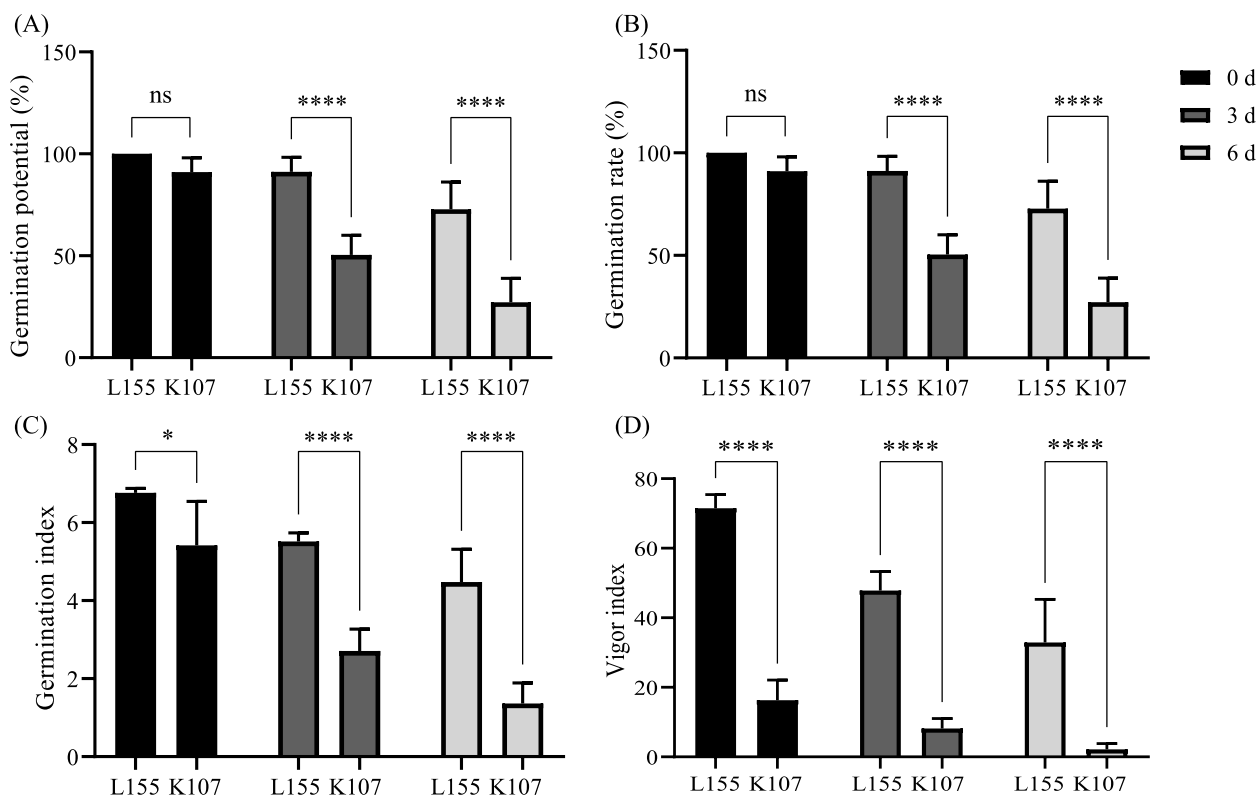


Fig. 1 GP, GR, GI, and VI of L155 and K107 at 0, 3 and 6 days after artificial aging treatments. **A** GP of L155 and K107 at 0, 3, and 6 days of artificial aging. **B** GR of L155 and K107 at 0, 3, and 6 days of artificial aging. **C** GI of L155 and K107 at 0, 3, and 6 days of artificial aging. **D** VI of L155 and K107 at 0, 3, and 6 days of artificial aging

On average, each sample yielded 48,979,461.78 high-quality clean reads, with an average of 33,790,087.83 reads being successfully aligned to the maize B73 V4.0 reference genome annotation. The average mapping rate of labeled reads to the B73 reference genome for L155 and K107 samples was 82.18% and 82.74%, respectively (Table S1). Principal component analysis of mRNAs and metabolites accurately divided all the samples into two different clusters, reflecting the obvious difference between K107 and L155 (Figure S1).

Validation of transcriptome data by qRT-PCR

To ensure the reliability of our transcriptome data, we randomly selected 9 differentially expressed genes for qRT-PCR analysis. The results illustrated the expression patterns of these genes across two lines at 0, 3, and 6 days following artificial aging. Remarkably, the expression patterns obtained through qRT-PCR closely matched those identified during RNA-seq analysis, thereby affirming the accuracy of our RNA-seq data (Figure S2).

Identification of differentially expression genes

Pairwise differential expression profile analysis (FDR ≤ 0.05 , $|\log_2FC| \geq 1.0$) was conducted across all time points to discern the differentially expressed genes during artificial aging (Fig. 2A). A total of 1,035 and 1,586 DEGs were identified in L155 and K107, respectively (Table S2, 3). When comparing consecutive time points, the majority of DEGs were observed between 0 and 6 d in L155, whereas in K107, most DEGs were found between 3 and 6 d, with a limited number of DEGs between 0 and 3 d. Notably, the 3 d vs 6 d comparison of L155 revealed the fewest differentially expressed genes, only one was detected, suggesting a slower rate of DEG expression change in L155 compared to K107. Moreover, there were 118 common DEGs in L155 and K107, while 917 DEGs were specific to the aging-tolerant line L155 (Table S4, Fig. 2C). Interestingly, both lines exhibited an increase in the number of up-regulated and down-regulated DEGs over time (Fig. 2A).

Identification and enrichment analysis of core DEGs

Remarkably, there exists an overlap of 118 DEGs common to both inbred lines, as portrayed in Fig. 2C

(Table S4). We considered these shared DEGs as "core DEGs" pivotal for the artificial aging tolerance of sweet corn seeds, possibly essential for their response to artificially induced accelerated aging. Of the 118 core DEGs, there were 9 mitochondrial genes and 12 transcription factors. To gain further insights into the functions and pathways associated with these core DEGs throughout seed aging, we performed GO and KEGG enrichment analyses for the 118 common DEGs, respectively (Figure S3a, b). Given the limited number of core DEGs, no significant KEGG pathway enrichment was observed. The GO analysis revealed that 118 DEGs were enriched in terms such as purine ribonucleoside monophosphate metabolic process, ribonucleoside triphosphate metabolic process, purine ribonucleoside triphosphate metabolic process and ATP metabolic process, encompassing a total of 45 terms, and most of which were related to energy metabolism (Figure S4).

Identification of continuously DEGs in K107 and L155

Since not all core genes responsive to artificial aging exhibit differential expression at all three time points, we focused on genes with continuously differential expression across all three time points (0 vs 3 days, 0 vs 6 days, and 3 vs 6 days). No common continuously DEGs were detected in L155 and K107. We then concentrated on the commonly DEGs in the 0 vs 3 days and 0 vs 6 days comparisons. Only 14 genes overlapped between the two datasets (Fig. 3A, B, C). Among these, Aquaporin PIP1 -5 (*Zm00001 d051872*) and Farnesylated protein 2 (*Zm00001 d034978*) showed higher expression levels in L155.

Transcriptomic changes of DEGs at different time points

As depicted in Fig. 1, following 3 and 6 days of artificial aging, the seed vigor indices of both lines decreased. To comprehensively grasp the global transcriptomic alterations during artificial aging, MapMan software [26] was utilized to identify metabolic pathways and biological processes at these two time-points, thereby visualizing the overall transcriptomic changes. During the early phase of artificial aging (0–3 days), K107 exhibited only a limited number of transcriptional changes. Specifically, there was upregulation in cell wall metabolism, aldehyde detoxification, the tricarboxylic acid (TCA) cycle, and photorepiration (Fig. 4A). In contrast, in the comparison

(See figure on next page.)

Fig. 2 Summary of changes in transcriptome and metabolite abundance in sweet corn seeds under artificial accelerated aging. **A, B** Summary of significant changes in the number of transcripts and metabolites between different time points. **C, D** Venn diagrams depicting Differentially Expressed Genes (DEGs) and Differentially Expressed Metabolites (DEMs) in L155 and K107. **E** Proportional representation of 100 core metabolites out of the total metabolites. **F** Detailed enumeration of the quantity and proportion of 100 core metabolites among various metabolites and their derivatives. **G** Classification of 536 metabolites

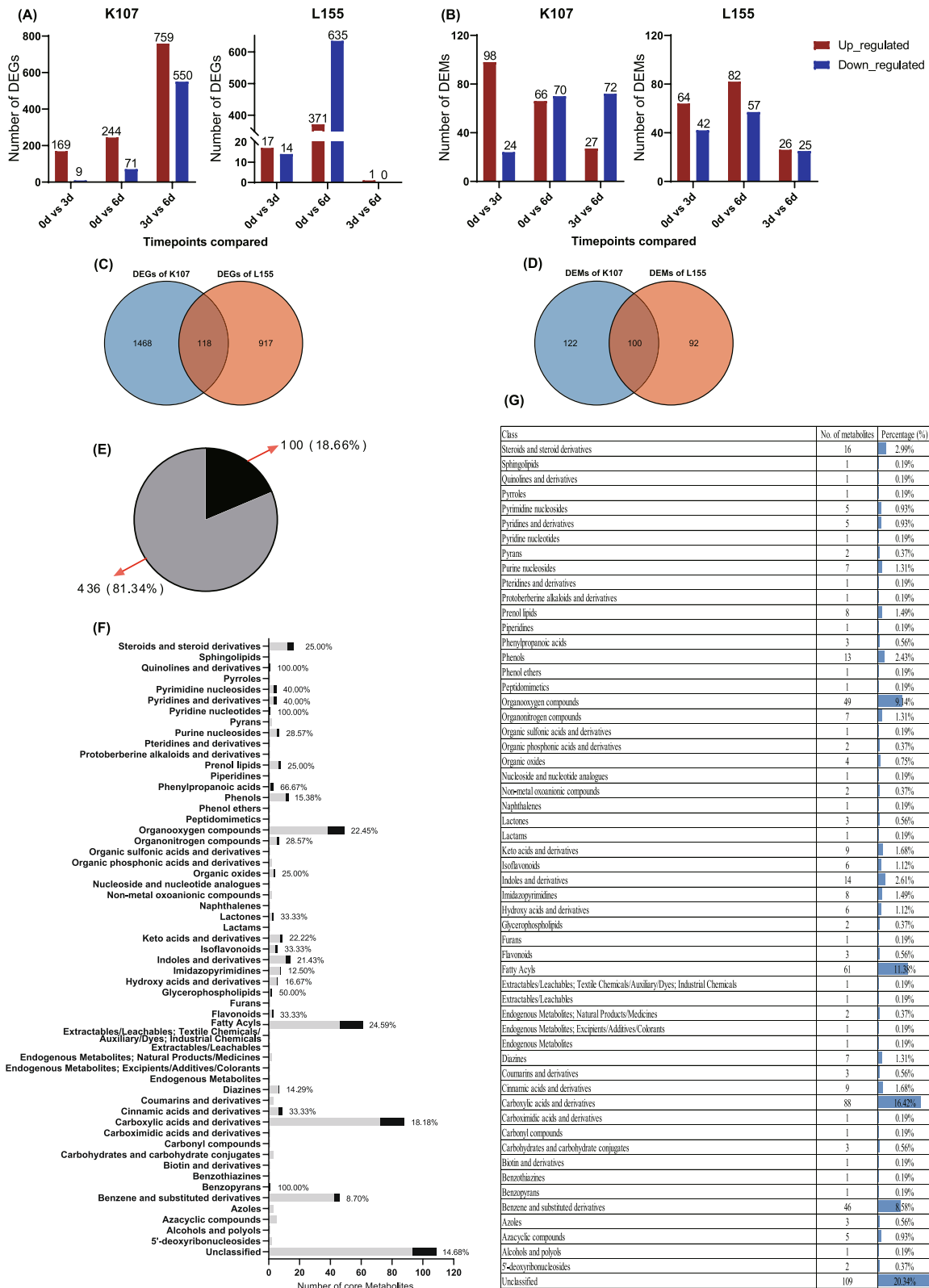


Fig. 2 (See legend on previous page.)

of 0 d vs 3 d, L155 showed upregulation solely in the phenylpropanoid and phenolics metabolic pathways (Figure S5a). Notably, when comparing 3 d vs 6 d in K107 and 0 d vs 6 d in L155, similar transcriptional changes were observed. These included upregulation in multiple categories such as cell wall, lipid metabolism, minor carbohydrate (CHO) metabolism, the TCA cycle, the Ascorbate/Glutathione cycle, fermentation, light-dependent reactions, photorepiration, and tetrapyrrole synthesis (Fig. 4B; S5b). Nevertheless, in the 3 d vs 6 d comparison for K107, the DEGs associated with the amino-acid metabolic pathway were only slightly up-regulated (Fig. 4B).

Enrichment of DEGs at different time points

To further clarify the transcriptomic changes at different time points, we carried out KEGG enrichment analyses on the DEGs in pairwise comparisons across three time points for two sweet corn lines (Fig. 5). All enrichment analyses were performed with a false discovery rate (FDR) threshold set at less than 0.05. The KEGG analysis results indicated that in the K107 line, a total of 13 enriched terms were detected across the three comparison groups. The 3 d vs 6 d comparison group had the largest number of KEGG pathways. In the L155 line, 14 enriched pathways were identified across the three comparison groups, with the 0 d vs 6 d comparison group, related to artificial aging, showing the highest number of KEGG pathways (Fig. 5).

In the 0 d vs 3 d comparison group, the DEGs in both K107 and L155 were significantly enriched in five pathways: Tryptophan metabolism, Benzoxazinoid biosynthesis, Oxidative phosphorylation, Glutathione metabolism, and Plant hormone signal transduction. Among these, Oxidative phosphorylation was the only common metabolic pathway shared by the two lines. For the 3 d vs 6 d comparison group, both lines exhibited significant enrichment in 10 metabolic pathways, yet no common pathway was found between them. Regarding the 0 d vs 6 d comparison group, both lines demonstrated significant enrichment in 13 pathways, with three common enriched pathways: Butanoate metabolism, Pyruvate metabolism, and Starch and sucrose metabolism. Notably, the 3 d vs 6 d comparison group for K107 and the 0 d vs 6 d comparison group for L155 had exactly the same enriched KEGG pathway.

Furthermore, GO enrichment analysis was conducted for the DEGs between different time points (Table S5,

6). In the K107 line, the DEGs from the 0 d vs 3 d, 0 d vs 6 d, and 3 d vs 6 d comparison groups were enriched in 141, 126, and 59 GO terms respectively (Table S6). In the L155 line, the corresponding DEGs were enriched in 63, 220, and 102 GO terms respectively (Table S6). In the 0 d vs 3 d comparison group for K107 and L155, a total of 34 common GO terms were enriched. Among them, GO:0055114 (oxidation–reduction process) was associated with ROS reduction. For the 0 d vs 6 d comparison group, six common GO terms were enriched, including GO:0043169 (cation binding), GO:0009266 (response to temperature stimulus), GO:0046872 (metal ion binding), GO:0009628 (response to abiotic stimulus), GO:0035251 (UDP-glucosyltransferase activity), and GO:0009408 (response to heat), suggesting their involvement in the response to artificial seed aging. Finally, in the 3 d vs 6 d comparison group, only two common enriched GO terms were observed, specifically related to cation binding (GO:0043169) and metal ion binding (GO:0046872).

Identification and enrichment of DEGs between K107 and L155

The seed vigor indexes of K107 and L155 exhibit substantial differences. Consequently, we centered our focus on the transcriptional patterns between K107 and L155 during artificial aging to probe into the underlying reasons for seed artificial aging. In the context of the transcriptome, we detected the highest number of DEGs on day 0, with a total of 2300 DEGs identified. The numbers of DEGs on day 3 and day 6 were 1668 and 2123, respectively (Fig. 6A). A greater proportion of DEGs displayed down-regulated expression. This indicates that, on the 3rd and 6th days after artificial aging, the expression of DEGs in L155 was significantly higher compared to that in K107 (Fig. 6A, B).

We conducted KEGG enrichment analysis for the DEGs at 0, 3, and 6 days after artificial aging. The analysis revealed 5 enriched pathways at 0th and 6th day, with no significantly enriched pathway detected at 3th day (Fig. 6C). On day 0, the DEGs between the two lines were enriched in Terpenoid backbone biosynthesis and Ribosome pathways. Meanwhile, the DEGs on day 6 were enriched in Sulfur metabolism, Linoleic acid metabolism, and Plant hormone signal transduction pathways. These results imply that these 5 pathways might play a role in contributing to the differences in artificial aging tolerance observed between K107 and L155.

(See figure on next page.)

Fig. 3 Identification of consecutive differentially expressed genes (DEGs) and metabolites (DEMs). **A** Venn diagram of DEGs at three time points for K107. **B** Venn diagram of DEGs at three time points for L155. **C** Heatmap depicting 14 consecutive DEGs, with gene expression standardized using z-score method; red represents high expression, while blue represents low expression. **D** Venn diagram of DEMs at three time points for K107. **E** Venn diagram of DEMs at three time points for L155. **F** Classification and content analysis of corresponding metabolites, two shared metabolites highlighted in red

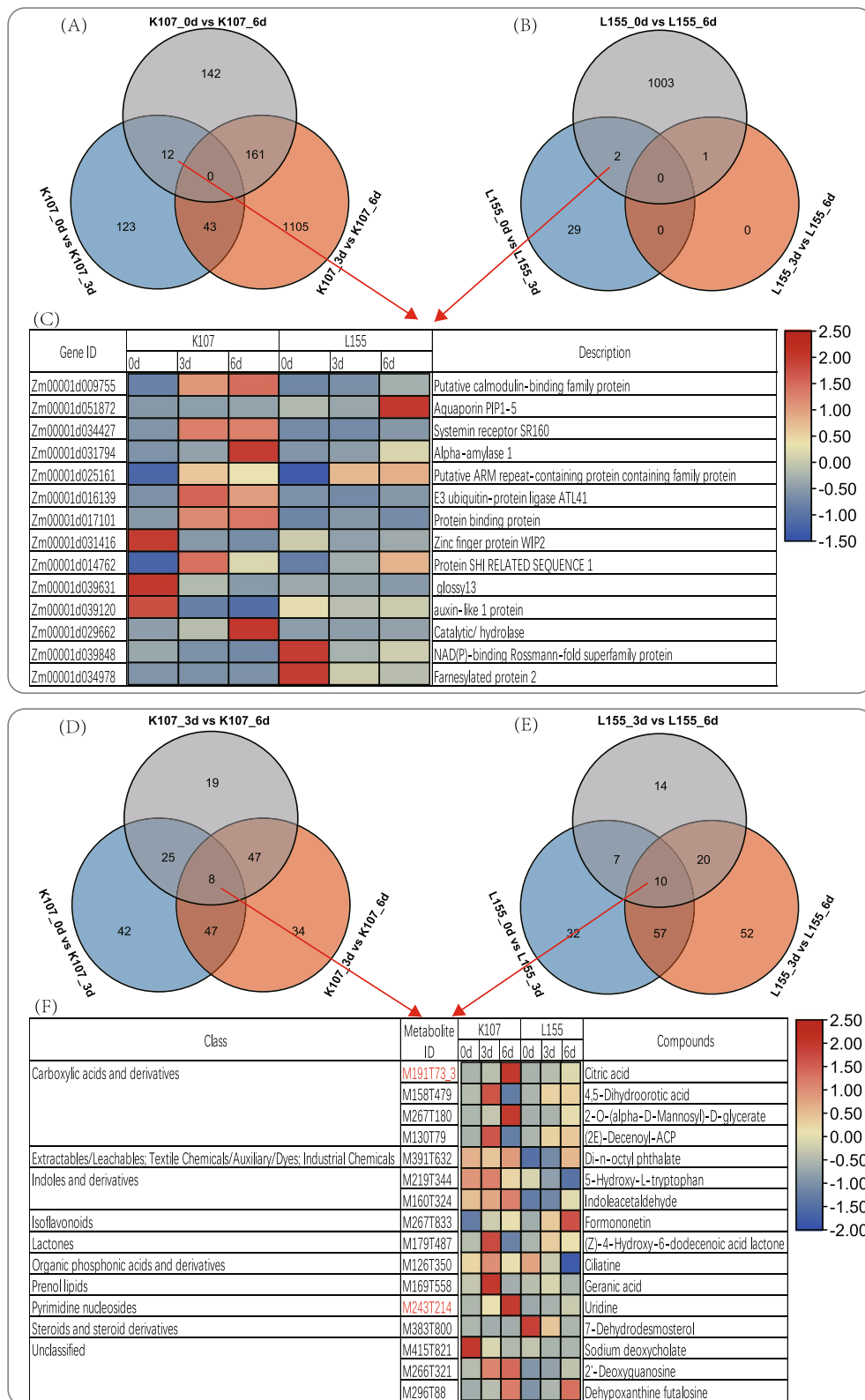


Fig. 3 (See legend on previous page.)

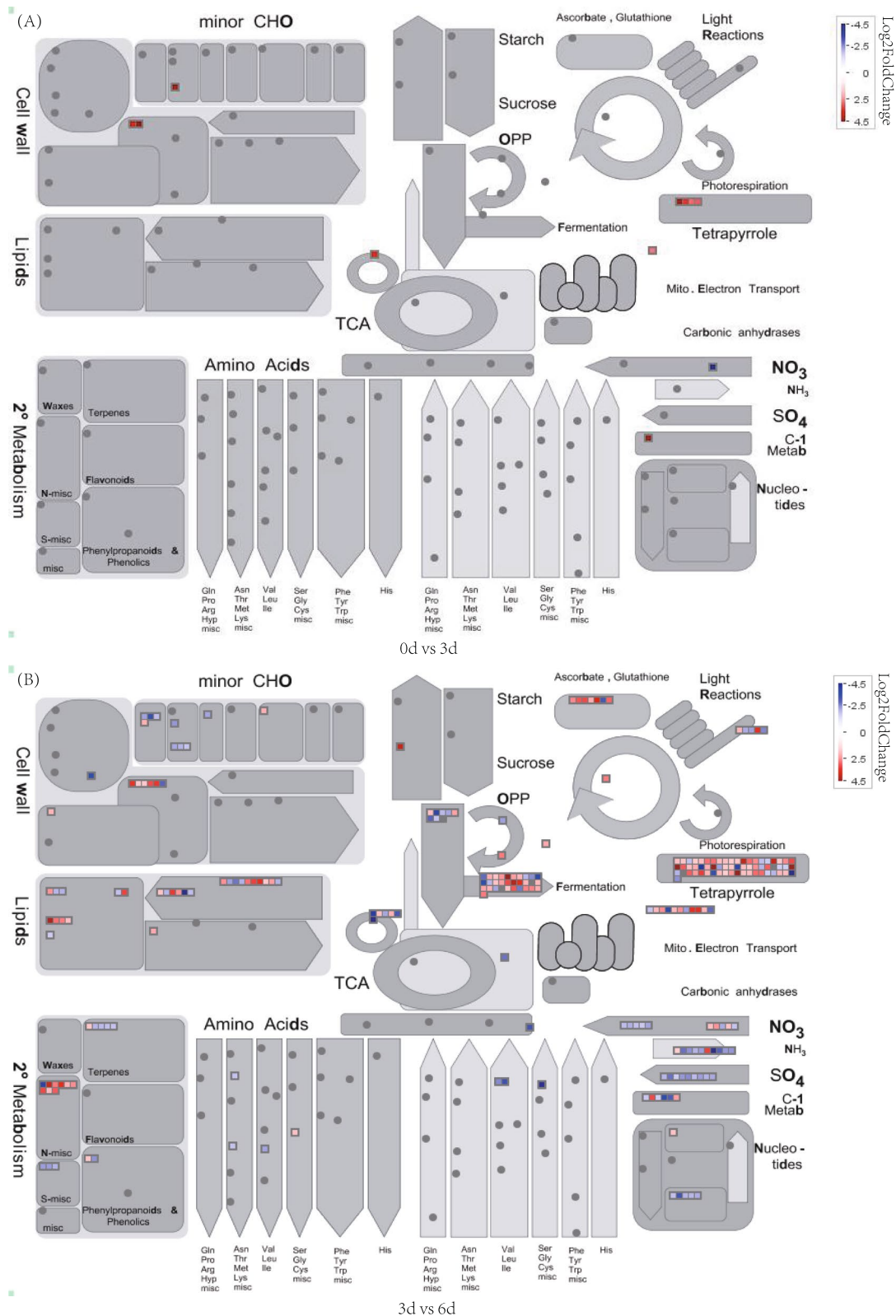


Fig. 4 The MapMan metabolic overview portrays the transcriptional differences during the artificial aging process of K107 seeds. **A** 0 vs 3 days. **B** 3 vs 6 days. The Log₂ FoldChange were based on three replicates. The color scale for Log₂ FoldChange ranges from – 4.5 to 4.5, where blue represents downregulated transcripts and red represents upregulated transcripts

KEGG B class	K107			L155			Pathway
	0d vs 3d	0d vs 6d	3d vs 6d	0d vs 3d	0d vs 6d	3d vs 6d	
Amino acid metabolism						5.04E-03	Alanine, aspartate and glutamate metabolism
	1.63E-03						Tryptophan metabolism
Biosynthesis of other secondary metabolites		5.07E-03		5.07E-03		2.91E-02	Benzoxazinoid biosynthesis
						7.23E-03	Phenylpropanoid biosynthesis
Carbohydrate metabolism			1.19E-05	1.19E-05		4.03E-05	Butanoate metabolism
			1.03E-02	1.03E-02			Galactose metabolism
			1.47E-02	1.47E-02			Glycolysis / Gluconeogenesis
			4.22E-02	4.22E-02	2.88E-02		Pyruvate metabolism
			2.68E-02	2.68E-02	7.23E-03		Starch and sucrose metabolism
Energy metabolism	6.28E-09	9.39E-06		9.39E-06			Oxidative phosphorylation
Glycan biosynthesis and metabolism						2.88E-02	Mannose type O-glycan biosynthesis
Lipid metabolism			3.91E-02	3.91E-02			alpha-Linolenic acid metabolism
			1.47E-02	1.47E-02			Fatty acid degradation
Metabolism of other amino acids						3.87E-02	Cyanoamino acid metabolism
	1.54E-05						Glutathione metabolism
Signal transduction			3.82E-02	3.82E-02			MAPK signaling pathway - plant
	2.74E-02						Plant hormone signal transduction



Fig. 5 KEGG enrichment analysis of DEGs in K107 and L155 (0 vs 3 days, 0 vs 6 days, 3 vs 6 days). Various colors represent FDR values, while blanks indicate no significant pathways during this period

Identification of differentially expressed metabolites

In the metabolite profiling analysis, 5 replicates were conducted at each time point, resulting in a total of 30 samples. A total of 536 metabolites were identified, including 57 compounds and their derivatives (Fig. 2E, g, Table S7). As with the transcriptome, pairwise analyses were conducted for all time points. Specifically, 222 and 192 differentially expressed metabolites (DEMs) were identified in K107 and L155, respectively (Table S8, 9). Over time, the number of up-regulated DEMs in K107 displayed a declining trend, while the number of down-regulated DEMs exhibited an increasing trend. Additionally, in the comparison group of 0d vs 6d in L155, both up and down-regulated DEMs were observed at their highest levels (Fig. 2B).

Identification and enrichment analysis of core DEMs

There is also an overlap of 100 DEMs in two lines, as shown in Fig. 2D (Table S10). We regarded these shared DEMs as "core DEMs" crucial for the artificial aging tolerance of sweet corn seeds. The 100 core metabolites constituted 18.66% of the total metabolites, encompassing 27 out of 57 identified classifications (Table S10). This subset comprised predominantly of Carboxylic acids and derivatives, Fatty Acyls, and Organooxygen compounds, with 16, 15, and 11 occurrences respectively, forming the majority among core metabolites (Fig. 2F, Table S10). KEGG analysis of 100 common metabolites identified

enrichment in a single term-Linoleic acid metabolism (Table S11).

Identification of continuously DEMs in the two lines

Similarly, for metabolites, we focused on those with continuously differential expression across the three time points. We identified 10 and 8 continuously DEMs in L155 and K107, respectively (Fig. 3D, E, F). A total of 16 continuously DEMs belonging to 10 classifications (Fig. 3F), with the highest representation found in the class of Carboxylic acids and derivatives, including Citric acid, 4,5-Dihydroorotic acid, 2-O-(α -D-Mannosyl)-D-glycerate, and (2E)-Decenoyl-ACP. A total of 7 metabolites were observed with continuously increasing abundance in both lines, with two shared metabolites highlighted in red: Citric acid and Uridine (Fig. 3F). These metabolites exhibited sustained differential expression in both lines and may be crucial in response to artificial aging.

Identification and enrichment of DEMs between K107 and L155

A total of 312 DEMs were detected in this study. Specifically, 201, 184, and 174 DEMs were identified at 0, 3, and 6 days after artificial aging, respectively (Fig. 7A, B). Among the metabolites, the most abundant ones included glutathione, adenosine, trehalose, and 10e,12z-octadecadienoic acid. KEGG enrichment analysis was

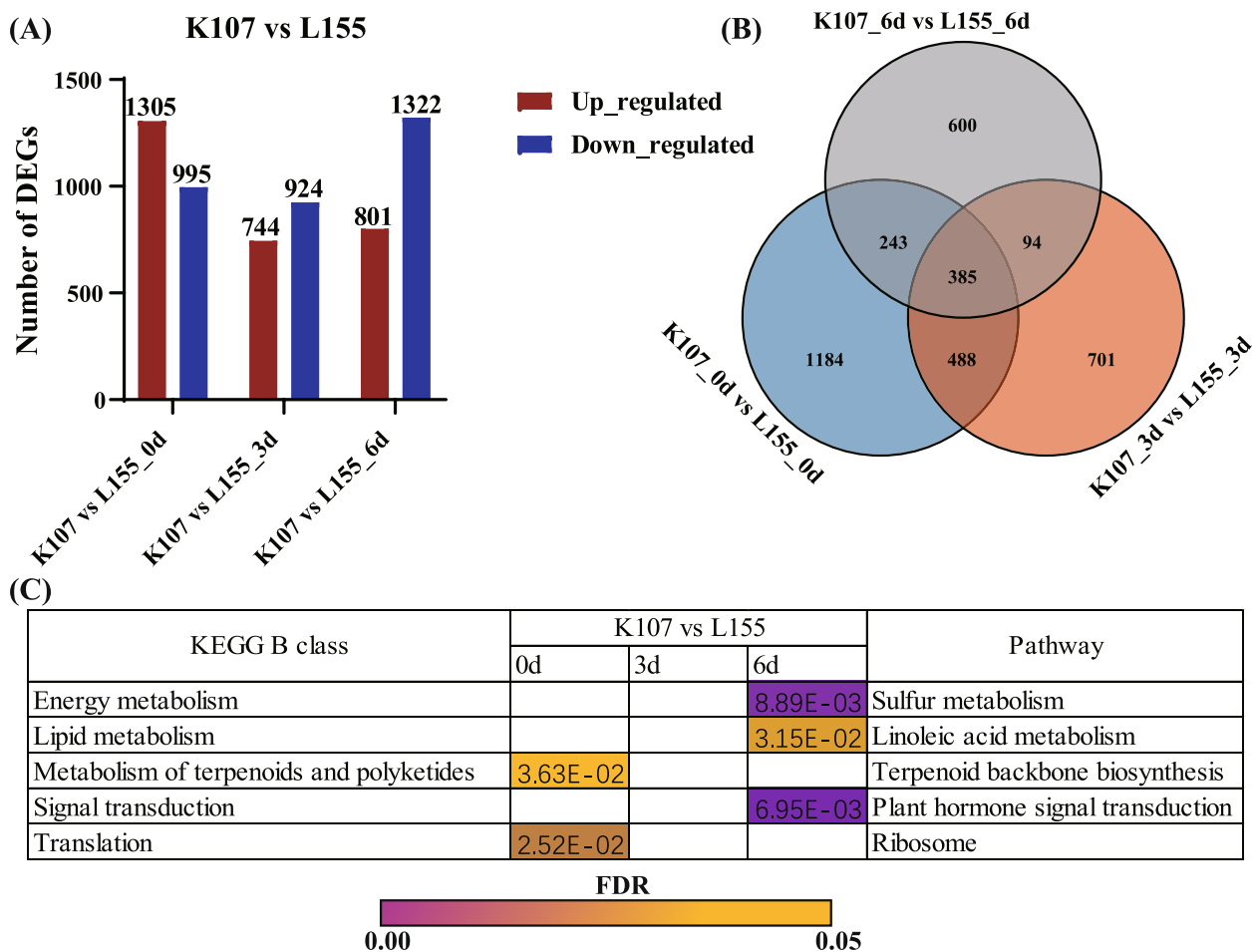


Fig. 6 The number of DEGs and KEGG enrichment analysis of K107 and L155 at 0, 3 and 6 days after artificial aging. **A** Upregulated and downregulated genes detected between K107 and L155. **B** Venn diagram showing the DEGs between K107 and L155 at 0, 3 and 6 days after artificial aging. **C** KEGG enrichment analysis of DEGs in K107 and L155 at 0, 3 and 6 days after artificial aging

conducted and the results revealed that two significant pathways were enriched. No significantly enriched pathways were detected at 0 day after treatment. At 3 days after treatment, the DEMs were enriched in the ABC transporters and linoleic acid metabolism pathways. At 6 days after treatment, the DEMs were enriched in the ABC transporters pathway. Notably, the ABC transporters pathway was the common enriched pathway. Comparing the KEGG enrichment analysis of DEMs with that of DEGs, a common enriched metabolic pathway, Linoleic acid metabolism, was detected.

AsA-GSH cycle unraveling the seed aging tolerance in K107 and L155

In the plant antioxidant system, the AsA-GSH cycle plays a fundamental and pivotal role in scavenging ROS. KEGG enrichment analysis indicated that the glutathione metabolism pathway likely mediates the differences in seed aging tolerance between K107 and L155. Therefore,

we focused on the changes in AsA-GSH cycle-related genes and metabolites (Fig. 8).

The DEGs within the glutathione pathway were screened out in this study. These DEGs include 14 *GST* genes, 3 *glutathione peroxidase (GPX)* genes, 3 *dehydroascorbate reductase (DHAR)* genes, and 3 *ascorbate peroxidase (APX)* genes (Fig. 8A, B, C, D, E, F, G). A total of 11 *GST* genes, except *Zm00001 d029707*, *Zm00001 d034937*, and *Zm00001 d043795*, showed higher expression in L155 than in K107. Among the 3 *GPX* genes and 3 *APX* genes, *Zm00001 d026154* and *Zm00001 d016802* had higher expression in L155, while *Zm00001 d051392* and *Zm00001 d003643* were highly expressed in K107. Additionally, *Zm00001 d002704* showed high expression in L155 at 0 day after artificial aging treatment and in K107 at 6 days after treatment, while *Zm00001 d028709* exhibited high expression in K107 at 6 days after treatment. The DEGs for both *DHAR* and *monodehydroascorbate reductase (MDHAR)* were highly expressed in K107.

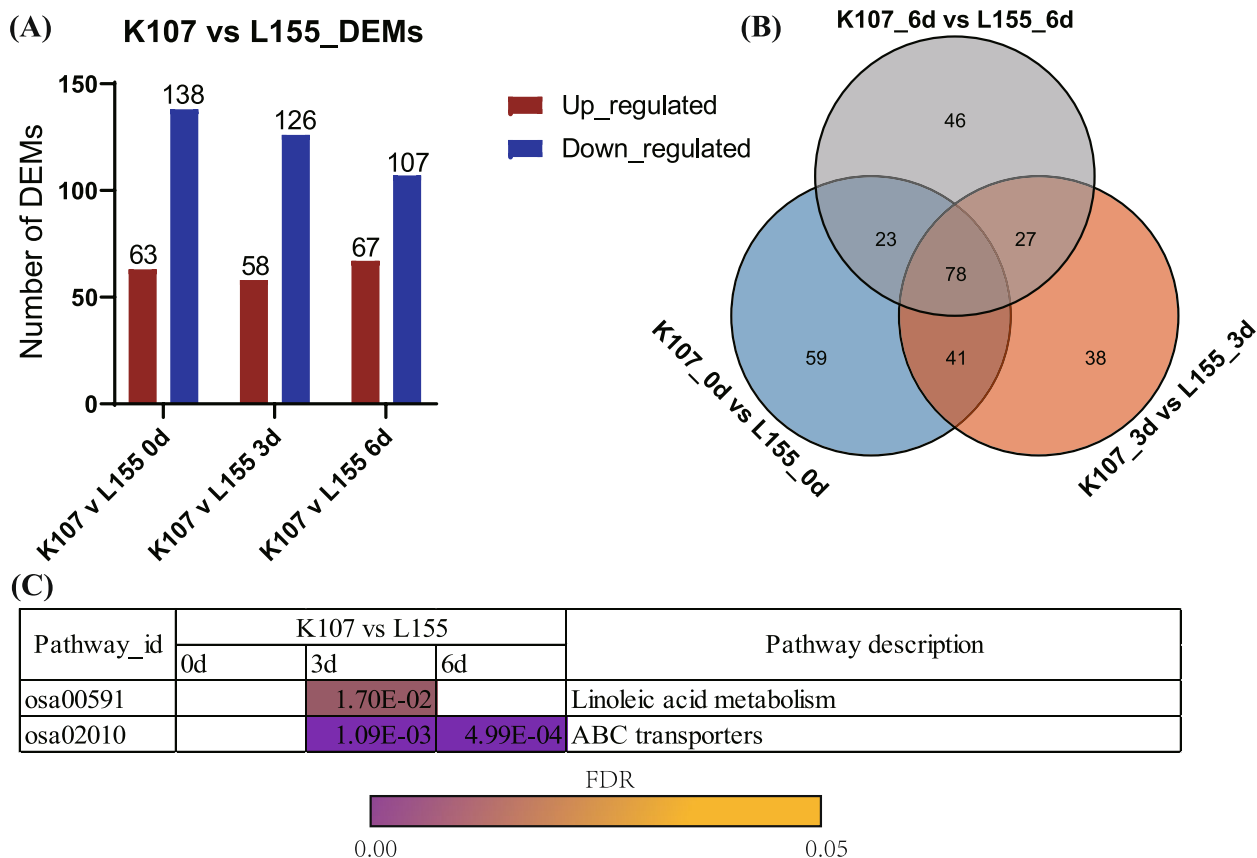


Fig. 7 The number of DEMs and KEGG enrichment analysis of K107 and L155 at 0, 3 and 6 days after artificial aging. **A** Upregulated and downregulated metabolites detected between K107 and L155. **B** Venn diagram showing the DEMs between K107 and L155 at 0, 3 and 6 days after artificial aging. **C** KEGG enrichment analysis of DEMs in K107 and L155 at 0, 3 and 6 days after artificial aging.

We further investigated 6 DEGs within *NADPH oxidase* gene family, all of which showed higher expression in K107 (Fig. 8G). Based on these findings, we propose that ROS production occurs early during artificial aging, with higher ROS production in K107, while superior ROS scavenging capabilities in L155.

In this study, our metabolite profiling detected both GSH and GSSG. The GSH content in K107 increased rapidly from 0 to 3 days and then decreased from 3 to 6 days, while in L155, the change was more gradual (Fig. 8H). These findings suggest that GSH content are affected by seed aging. The changes in GSH and GSSG content in K107 were significantly faster than those in L155. Thus, we hypothesize that the ROS-scavenging capacity of L155 is superior to that of K107, which is consistent with the differences in seed vigor observed after artificial aging treatment. In summary, the variation in ROS production and scavenging capacity is considered as a crucial factor contributing to the contrasting seed aging tolerance observed in K107 and L155.

Discussion

This study conducted a comprehensive analysis of the transcriptome and metabolome during the aging process of sweet corn seeds. In our study, the maximum change in transcriptional level in K107 occurred in the 3 d vs 6 d comparison group, while in L155, it occurred in the 0 d vs 6 d comparison group. In L155, the transcript response is delayed as compared to K107. In contrast, the differences in metabolite abundance for both inbred lines occurred in the 0d vs 6d comparison group, differing from the changes in transcriptional data. Howell et al. [27] investigated the changes in embryonic transcript and metabolite abundance within 48 h after imbibition of rice seeds. In their research, they suggested that early changes in metabolites derive from the activity of pre-existing enzymes and the late changes in metabolites are driven by transcription and translation. Our results indicate that changes in metabolites ensue subsequent to the changes in transcripts, consistent with previous research.

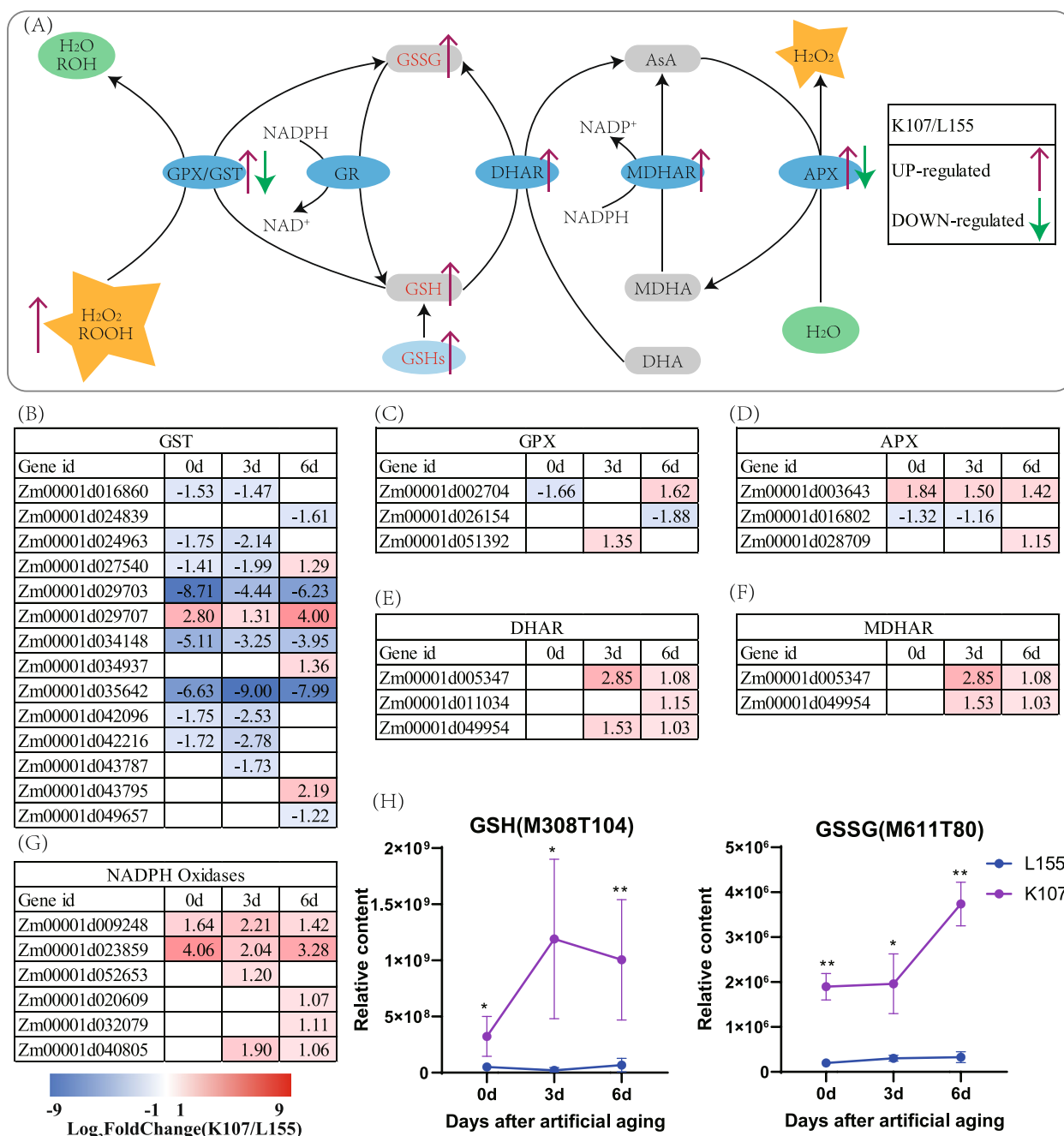


Fig. 8 Changes in AsA-GSH cycle-related genes and metabolites. **A** AsA-GSH pathway model. Red arrows indicate upregulated expression, while blue arrows indicate downregulated expression. **B, C, D, E, F, G** Log₂FC of 6 DEGs at day 0, 3, and 6 including GST, GPX, APX, DHAR and MDHAR. **H** Changes in reduced glutathione (GSH) content in K107 and L155. **I** Changes in reduced glutathione (GSH) content in K107 and L155

A total of 118 core DEGs were identified in this study, consisting of 9 mitochondrial genes and 12 transcription factors. These core DEGs are highly likely to form the core of the response mechanism of sweet corn seeds to artificial aging stress, which are key genes for seeds to maintain their viability. Mitochondria, the

energy-producing factories of cells, are of great significance in the physiological activities of seed germination [28]. It is believed that ROS-related mitochondrial dysfunction plays a crucial role in seed deterioration [29]. Additionally, transcription factors can regulate the expression of other genes. The differential expression of

transcription factors implies that there may be a series of changes in the expression of downstream genes. These changes may involve multiple physiological processes, such as stress responses and metabolic regulation, thereby affecting the seeds' tolerance to artificial aging [30]. GO analysis shows that these 118 DEGs are significantly enriched in 45 terms related to energy metabolism. During seed deterioration, the respiratory pattern is complex and varied, and the deterioration rate of embryo and endosperm is different [31]. In conclusion, these core DEGs provide important clues for further understanding the tolerance mechanism of sweet corn seeds to artificial aging.

In the germination process of rice seeds, a large number of transcripts are involved in cell wall metabolism, lipid metabolism, nucleotide degradation, amino acid synthesis, TCA cycle, and jasmonic acid biosynthesis [27]. Yang et al. [32] also observed several other upregulated pathways, such as light reaction, photorespiration, mitochondrial electron transport, tetrapyrrole synthesis, and amino acid synthesis. Our MapMan analysis revealed that early DEGs during artificial aging were only enriched in a few metabolic pathways including cell wall metabolism, lipid metabolism, nucleotide degradation etc. (Fig. 4, S5), which were part of previous studies. In previous study, a lipoprotein gene (*GRMZ2G044627*) and *ZmLOX1* within QTLs for seed vigor involved in lipid metabolism [13, 15]. We also identified variances in the transcriptomic alterations between K107 and L155, notably observing a more pronounced delayed transcriptional response in the aging-tolerant line.

A total of 14 continuously DEGs were identified, and among these 14 continuously expressed DEGs, two genes, *Aquaporin PIP1 -5* (*Zm00001 d051872*) and *Farnesylated protein 2* (*Zm00001 d034978*), showed higher expression levels in L155. *Aquaporin OsPIP1* has been demonstrated to promote salt resistance and seed germination in rice [33], while *ZmRAFS* has been associated with seed aging tolerance in maize [22]. KEGG and GO enrichment analyses were carried out on all DEGs in pairwise-comparison groups at three time points. The K107 3 d vs 6 d comparison group had identical enriched KEGG pathways as the L155 0 d vs 6 d comparison group. These pathways are associated with carbohydrate metabolism, lipid metabolism, and signal transduction. The findings suggest that the transcriptional alterations caused by artificial aging are consistent, although not synchronized, across different materials. Furthermore, carbohydrate and lipid metabolism may play a role in the tolerance to seed aging. In rice, the enrichment of DEGs in the seed embryos of two species varied at different aging time points under accelerated aging [34]. In this study, the common

enriched KEGG term of the 0 d vs 3 d group was oxidative phosphorylation. During seed deterioration, oxidative phosphorylation serves as an important source of ROS within cells [7]. The accumulation of ROS in the mitochondria reduces the activity of the antioxidant system.

The KEGG enrichment results offer valuable insights into the potential molecular mechanism of tolerance to artificial aging between K107 and L155. At 0 day after treatment, the DEGs were enriched in the terpenoid backbone biosynthesis and ribosome pathways (Fig. 6). Terpenoids are involved in diverse biological functions, including plant defense and stress response [35]. The enrichment of the Ribosome pathway might suggest differences in the basal translation machinery or the capacity to rapidly synthesize proteins, which could be essential for cells to adapt to the stress of artificial aging. The ribosome and peroxisome pathways were enriched in response to seed aging in sweet corn [24].

At 6 days after treatment, the enrichment of DEGs were sulfur metabolism, linoleic acid metabolism, and plant hormone signal transduction. Sulfur metabolism is involved in the synthesis of crucial molecules like glutathione, a key antioxidant [36–38]. In cotton, the linoleic acid content in the RNAi-mediated transgenic strain of two genes, *GhFAD2 -1* and *GhFATB*, decreased by 33.92%, leading to a decline in seed germination potential and vigor, especially under cold stress conditions [39]. Linoleic acid metabolism is associated with enhanced seed vigor in chia seeds [40]. Plant hormone signal transduction pathways play a vital role in regulating plant growth, development, and stress responses. Hormones such as abscisic acid, ethylene, and auxin can modulate various physiological processes in response to stress [41, 42]. Overall, these five pathways (terpenoid backbone biosynthesis, ribosome, sulfur metabolism, linoleic acid metabolism, and plant hormone signal transduction) likely interact intricately to contribute to the observed differences in artificial aging tolerance between K107 and L155. Further exploration of the specific genes and molecular mechanisms within these pathways is necessary to fully comprehend the molecular mechanism of aging-tolerance in sweet corn.

A total of 16 consecutive DEMs were identified in K107 and L155. Among the 16 consecutive DEMs, one isoflavone, Formononetin, exhibited an increase in abundance during artificial aging treatment in both lines, with a more obvious increase in the seed aging-tolerant line L155. Dong et al. [43] found that there were 10 flavonoid compounds with higher contents in germinating seeds than in grains, suggesting an increased synthesis of

flavonoids during seed germination. These results suggest that isoflavone may also be involved in seed aging tolerance.

The increase of 2'-Deoxyguanosine content was also detected following artificial aging treatment in this study. The accumulation of DNA damage during seed aging is a major cause of chromosomal aberrations [44]. Generally, ROS are the main triggers for DNA strand breaks, either by directly causing deoxygenation of the deoxyribose unit or possibly through covalent modification of bases [45]. One primary modification is hydroxylation at the C-8 position of guanine, leading to the generation of 8-hydroxy-2'-deoxyguanosine (8-OHdG) [5, 45]. The increase of 2'-deoxyguanosine content meant that the genetic material of the seeds was damaged.

Due to the varying genetic backgrounds, the DEGs and DEMs we screened may potentially be false positives. However, it is also noteworthy that because of the differences in the genetic background, we were able to identify more valuable target genes and metabolites [32, 39, 46, 47]. Based on our results, it is believed that the screened DEGs and DEMs are quite reliable, as they have identified key genes and metabolites related to seed vigor reported by previous studies. In summary, these 14 consecutive DEGs and 16 DEMs serve as ideal candidate biomarkers during the seed aging process in sweet corn.

ROS are inevitable by-products of aerobic metabolism. An increasing body of evidence [5, 7, 28] points to the crucial role of ROS in the processes of seed aging. The accumulation of ROS during seed deterioration has been reported in diverse plant species [10, 21, 48]. Glutathione has the capacity to scavenge ROS either directly or indirectly. This fact brought our interest in further exploring the ascorbate–glutathione pathway. In our study, the alterations in GSH and GSSG levels indicated that both lines suffered oxidative stress (Fig. 8H). Moreover, we probed deep into the key genes involved in ROS production and the AsA-GSH cycle. Six differentially expressed *NADPH* genes were highly expressed in K107. In contrast, the majority of *GST* genes showed higher expression levels in L155. Yang et al. [32] investigated the ROS-scavenging ability mediated by certain *APX*, *GPX*, and *GST* genes, which were associated with the germination and seedling growth rates between indica and japonica rice. As reported in oat seed aging, the AsA-GSH cycle initially alleviates H_2O_2 but its inactivity later limits scavenging of ROS, spotlighting its crucial role in seed vigor [10]. In our findings, the lower expression of *NADPH* genes in L155 led to reduced ROS production. Additionally, the differential expression level of *GST* genes was the main cause of the difference in ROS scavenging capabilities. These genes, which are differentially expressed in ROS production and scavenging processes,

ultimately influenced the difference in seed aging tolerance in sweet corn.

Conclusions

This study represents the first to investigate the global transcriptional and metabolic profiles of sweet corn subjected to artificial aging. We identified fourteen common transcripts and sixteen shared metabolites with sustained differential expression across both lines, which may play a critical role in the seed aging response. Enrichment analysis of DEGs revealed a complete overlap in KEGG pathways between the 3 d vs 6 d comparison of K107 and the 0 d vs 6 d comparison of L155, suggesting a delayed response in the sensitive line. Additionally, we explored transcriptomic and metabolomic differences under artificial aging treatment, identifying five significantly enriched KEGG pathways at 0, 3, and 6 days between K107 and L155, namely tryptophan metabolism, benzoxazinoid biosynthesis, oxidative phosphorylation, glutathione metabolism, and plant hormone signal transduction. A total of 312 DEMs at 0, 3, and 6 days after seed aging treatment were enriched in ABC transporters and linoleic acid metabolism pathways. The co-enriched pathway of DEGs and DEMs was linoleic acid metabolism. Moreover, a detailed AsA-GSH pathway examination revealed that ROS production mediated by *NADPH* and the scavenging capacity facilitated by *GST* are vital for seed aging tolerance.

Methods

Plant materials and treatment conditions

K107 and L155 were *sh₂sh₂* genotypes and obtained from South China Agricultural University. Previous research has identified K107 as a line sensitive to seed aging [24]. In contrast, L155, which was selected from the RIL population of K107 and K62, exhibited great tolerance to seed aging compared to K62 [25]. These lines were cultivated at the teaching and research base of South China Agricultural University in Guangzhou, China (113°E, 23°N) during the autumn of 2020. Seeds were harvested at physiological maturity, 45 days post-pollination, and were allowed to dry naturally. For the purpose of artificial accelerated aging, the seeds were placed in a seed aging chamber (LH-150S, Shanghai Qixin, Shanghai, China) set at a temperature of 41 °C and 100% relative humidity [24]. Seeds were collected at 0, 3, and 6 days after artificial accelerated aging treatment for RNA sequencing and metabolomic analysis.

The seed vigor of aged seeds was evaluated using the methodology outlined by Wang et al. [3] in a growth chamber maintained at 25 °C with a photoperiod of 16 h light and 8 h dark (Laifu, Ningbo, China). A total of

twenty-five seeds were placed in a germination box filled with 4 cm of moist quartz sand, which was then covered with an additional 2 cm of moist sand. Each experiment was replicated three times. The parameters assessed included GP, GR, GI and VI, calculated according to the procedures described by Guan et al. [49]. GP was determined as the germination rate on the fourth day. The GR was calculated using the formula: Germination rate = $n/N \times 100\%$, where n denotes the total number of seeds that germinated and N represents the total number of seeds assessed on the eighth day. The GI was computed with the formula: $GI = \sum Gt/Dt$, where Dt indicates the day of germination and Gt signifies the number of seeds that germinated on that day. The VI was determined using the equation: $VI = GI \times SW$, where SW refers to the fresh weight of seedlings measured on the eighth day.

RNA extraction, library preparation, and sequencing

RNA sequencing services were conducted by Personal Biotechnology Co., Ltd., located in Shanghai, China. Total RNA from each sample was homogenized in liquid nitrogen and extracted using the Trizol reagent kit (Invitrogen, Carlsbad, CA, USA) following the manufacturer's instructions. The quality of the RNA was evaluated using an Agilent 2100 Bioanalyzer (Agilent Technologies, Palo Alto, CA, USA) and further verified for integrity through RNase-free agarose gel electrophoresis (Figure S6). Each sample consisted of three biological replicates. Seeds collected at 0, 3, and 6 days after artificial aging treatment were utilized for total RNA extraction, library preparation, and quantitative real-time PCR analysis. The sequencing libraries were constructed following the methodology outlined by Wang et al. [24], resulting in a total of 18 mRNA-Seq libraries, which were sequenced on the Illumina HiSeqTM 4000 platform.

RNA sequencing data analysis

The quality assessment of clean reads was carried out using FastQC V0.11.9 (Illumina; <https://www.bioinformatics.babraham.ac.uk/projects/fastqc/>). High-quality reads with $Q > 20$ were aligned to the reference genome (*Zea_mays*. B73_RefGen_v4.dna.toplevel.fa), which was retrieved from the Plants Ensembl database (<http://www.Ensembl.org/>). To facilitate the alignment, the reference genome index was generated using Bowtie2 software [50]. Reads were then filtered with Tophat2 [51], and compared against the reference index. Gene function annotation was conducted based on multiple databases, including the Nucleotide Database (NT), Gene Ontology (GO), Enzyme Commission (EC), Kyoto Encyclopaedia of Genes and Genomes (KEGG), and Swiss-Prot. The read count for each gene was determined using HTSeq [52]. Expression levels were normalized to

reads per kilo bases per million reads (RPKM), with genes having RPKM values > 1 being considered as expressed [53]. After calculating the expression levels of transcripts and genes, the DESeq2 method (version 1.34.0) [54] was utilized for differential expression analysis. For statistical significance, a false discovery rate (FDR) threshold of ≤ 0.05 and $|\log_2 FC| \geq 1.0$ were applied to identify differentially expressed genes. For the DEGs, GO analysis was performed using topGO [55], while KEGG pathway analysis was carried out using KAAS [56]. Additionally, the transcriptome data was further analyzed using MapMan software (ver. 3.6.0RC1) [26] to map functional categories, perform time-course analyses, and identify significantly over-represented functional groups.

Metabolomic analysis

Metabolite profiling analysis was conducted by Suzhou PANOMIX Biomedical Tech Co., LTD (Suzhou, China) (<https://www.panomix.com/>) using a widely targeted metabolomics approach. The reagents and methods for metabolite extraction followed as described by Tan et al. [57]. All samples were analyzed using an ACQUITY UPLC system (Waters, Milford, MA, USA) equipped with an ACQUITY UPLC HSS T3 (150 mm \times 2.1 mm, 1.8 μ m, Waters) column, maintained at 40 °C. Flow rate and injection volume were set at 0.40 mL/min and 2 μ L, respectively. Analysis of samples was performed using both positive and negative ion modes. For positive mode, the mobile phase consisted of a solution of 0.1% formic acid in acetonitrile (v/v) (C) and 0.1% formic acid in water (v/v) (D). The following gradient was used: 0–1 min, 2% C; 1–9 min, 2–50% C; 9–12 min, 50–98% C; 12–13.5 min, 98% C; 13.5–14 min, 98–2% C; 14–20 min, 2% C. For negative mode, the mobile phase consisted of acetonitrile (A) and ammonium formate (B) (5 mmol L⁻¹). The following gradient was used: 0–1 min, 2% A; 1–9 min, 2–50% A; 9–12 min, 50–98% A; 12–13.5 min, 98% A; 13.5–14 min, 98–2% A; 14–17 min, 2% A. Quality control (QC) samples were run at the beginning, middle, and end of each batch.

Metabolite mass spectrometry detection was performed on a Q Exactive instrument (Thermo Fisher Scientific, USA) equipped with an ESI ion source. The spray voltages were set at 3.8 kV and – 2.5 kV for positive and negative modes, respectively. Both MS1 and MS/MS (full-scan MS-ddMS2 mode, data-dependent MS/MS) were acquired. Sheath gas and auxiliary gas were set at 45 and 15 arbitrary units, and the capillary temperature was set to 325°C. Orbitrap analyzer conducted full scans in the mass range of 81–1000 m/z (mass-to-charge ratio) at a mass resolving power of 70,000. High-energy collision-induced dissociation (HCD) scan was utilized for

data-dependent MS/MS experiments. Normalized collision energy was set at 30 eV, with a resolution of 70,000 full width at half maximum (FWHM) for MS1 and 17,500 FWHM for MS/MS. Dynamic exclusion was implemented to remove unnecessary information from the MS/MS spectra.

Mass spectrum data processing

The raw data were converted to the mzXML format using the MSConvert tool within the ProteoWizard software package (V3.0.8789), and subsequent peak identification, filtering, and alignment were conducted using the XCMS package. Default settings of XCMS included the following parameters: bw = 2, ppm = 15, peak width = c(5, 30), mzwidth = 0.015, mzdifff = 0.01, and method = "centWave". Metabolites were identified based on accurate mass (molecular weight error < 30 ppm) and matching MS/MS data against several databases including HMDB (<http://www.hmdb.ca>), MassBank (<http://www.massbank.jp/>), Lipid-Maps (<http://www.lipidmaps.org>), mzCloud (<https://www.mzcloud.org>), Metlin (<http://Metlin.screpps.edu>), as well as proprietary databases established by Suzhou PANOMIX Biomedical Tech Co., LTD (Suzhou, China). Following standardization, only ion peaks with a relative standard deviation (RSD) below 30% in QC samples were used for metabolite annotation.

The principal component analysis and orthogonal projection to latent structures discriminant analysis (OPLS-DA) were conducted for detecting significant differences in relative metabolite levels using the Ropl package (Analysis of the human adult urinary metabolome variations with age, body mass index, and gender by implementing a comprehensive workflow for univariate and OPLS statistical analyses). The variable importance in projection (VIP) value from the PLS-DA model was used as the discrimination parameter for the analysis of metabolites, aiding in the selection of indicative metabolites. MetaboAnalyst (<https://www.metaboolanalyst.ca/>) was utilized for enrichment analysis and pathways analysis of the selected differentially expressed metabolites (Using MetaboAnalyst 5.0 for LC–HRMS spectra processing, multi-omics integration and covariate adjustment of global metabolomics data). When *P* value < 0.05 and VIP > 1, the metabolites were considered to have statistical significance.

Quantitative real-time PCR

Nine DEGs were randomly selected for validation of the sequencing data through qRT-PCR analysis. Primers (Table S12) were designed using reference gene sequences with Primer 5.0 software. The internal reference gene for mRNA was UBQ7 [58]. Reverse transcription of mRNA was conducted using the FastKing gDNA Dispelling RT SuperMix (Generay Biotech Co., Ltd.)

according to the manufacturer's instructions. The first strand was synthesized using the miR-X miRNA First-Strand Synthesis Kit (Generay Biotech Co., Ltd.), and reverse transcription was performed using the cDNA Synthesis kit (TaKaRa, China). Quantitative PCR for mRNA was carried out using SYBR Green fluorescent dye (Beijing Qingke Biological Technology Co., Ltd.) and the miRcute Plus miRNA Fluorescence Quantitation Kit (Generay Biotech Co., Ltd.) on a fluorescence quantitative PCR instrument. Each sample was replicated three times, and the relative expression of DEGs was calculated using the $2^{-\Delta\Delta C_t}$ method [59].

Supplementary Information

The online version contains supplementary material available at <https://doi.org/10.1186/s12864-025-11586-x>.

Supplementary Material 1: Table S1. Summary of read mapping statistics.

Supplementary Material 2: Table S2. Lists of differentially expressed genes (DEGs) in K107. Table S3. Lists of differentially expressed genes (DEGs) in L155. Table S4. Intersection of DEGs in L155 and K107.

Supplementary Material 3: Table S5. GO analysis for the DEGs (0 v 3 days, 3 v 6 days, 3 v 6 days) in K107. Table S6. GO analysis for the DEGs (0 v 3 days, 3 v 6 days, 3 v 6 days) in L155.

Supplementary Material 4: Table S7. Detected metabolites and relative content. Table S8. All DEMs of K107. Table S9. All DEMs of L155. Table S10. Intersection of DEMs in K107 and L155.

Supplementary Material 5: Table S11. The KEGG enrichments of 100 common metabolites.

Supplementary Material 6: Table S12. Primers used for qRT-PCR analysis.

Supplementary Material 7: Figure S1. Principal component analysis (PCA) plot of the first two PCs of total DEGs (A) and DEMs (B).

Supplementary Material 8: Figure S2. qRT-PCR validation of DEGs.

Supplementary Material 9: Figure S3. GO (A) and KEGG (B) enrichment analyses for the 118 common DEGs.

Supplementary Material 10: Figure S4. The GO terms of biological process (BP) enriched by 118 common DEGs.

Supplementary Material 11: Figure S5. The MapMan metabolic overview portrays the transcriptional differences during the artificial aging process of L155 seeds. A, 0 vs 3 days. B, 0 vs 6 days.

Supplementary Material 12.

Authors' contributions

F.F. and P.L. designed the experiments, and they obtained funding for the research. Z.Z., R.Y. and F.F. contributed to compiling and analyzing the data and wrote the manuscript. L.G. and F.J. conducted the statistical analysis. S.H., Q.C. and Z.Z. performed the experimental analyses. All authors have read and agreed to the published version of the manuscript.

Funding

This research was supported by the National Natural Science Foundation of China (31871713), Guangzhou Science and Technology Plan (2024B03 J1303), Special Program for Key Fields of Natural Sciences in Ordinary Colleges and Universities in Guangdong Province (2023ZDZX4017), and Special Fund for Science and Technology Innovation in Yangjiang City, Guangdong Province (SDZX2023024).

Data availability

Sequence data that support the findings of this study have been deposited in the Sequence Read Archive with the primary accession code PRJNA1108064.

Declarations

Ethics approval and consent to participate

Not applicable.

Consent for publication

Not applicable.

Competing interests

The authors declare no competing interests.

Author details

¹College of Agriculture and Biology, Laboratory for Research and Development of Crop Germplasm Resources, Zhongkai University of Agriculture and Engineering/Guangzhou Key, Guangzhou 510225, China. ²College of Agriculture, Guangdong Provincial Key Laboratory of Plant Molecular Breeding, South China Agricultural University, Guangzhou 510642, Guangdong, China. ³Guangdong Agricultural Technology Extension Center, Guangzhou 510145, Guangdong, China.

Received: 7 May 2024 Accepted: 9 April 2025

Published online: 15 April 2025

References

- Revilla P, Anibas CM, Tracy WF. Sweet corn research around the world 2015–2020. *Agronomy*. 2021;11:534. <https://doi.org/10.3390/agronomy11030534>.
- Liu WN, Wang Z, Gan YY, Hu JG, Yin Y. Development situation and countermeasures of Guangdong sweet corn industry in 2015. *Guangdong Agric Sci*. 2016;43(3):5 <http://doi/CNKI:SUN:GDNY.0.2016-03-003>.
- Wang B, Yang R, Ji Z, Zhang H, Zheng W, Zhang H, et al. Evaluation of biochemical and physiological changes in sweet corn seeds under natural aging and artificial accelerated aging. *Agronomy*. 2022;12:1028. <https://doi.org/10.3390/agronomy12051028>.
- Li K, Huang C. Current production status, problem and counter measure on sweet corn industry in China. *Sugar Crops of China*. 2021;43:67–71.
- Ebone LA, Caverzan A, Chavarria G. Physiologic alterations in orthodox seeds due to deterioration processes. *Plant Physiol Bioch*. 2019;145:34–42. <https://doi.org/10.1016/j.plaphy.2019.10.028>.
- Sharma P, Jha AB, Dubey RS, Pessaraki M. Reactive oxygen species, oxidative damage, and antioxidative defense mechanism in plants under stressful conditions. *J Bot*. 2012;2012:1–26. <https://doi.org/10.1155/2012/217037>.
- Kurek K, Plitta-Michalak B, Ratajczak E. Reactive oxygen species as potential drivers of the seed aging process. *Plants*. 2019;8:174. <https://doi.org/10.3390/plants8060174>.
- Lin YX, Xu HJ, Yin GK, Zhou YC, Lu XX, Xin X. Dynamic changes in membrane lipid metabolism and antioxidant defense during soybean (*Glycine max* L. Merr.) seed aging. *Front Plant Sci*. 2022;13. <https://doi.org/10.3389/fpls.2022.908949>.
- Yin G, Xin X, Song C, Chen X, Zhang J, Wu S, et al. Activity levels and expression of antioxidant enzymes in the ascorbate–glutathione cycle in artificially aged rice seed. *Plant Physiol Bioch*. 2014;80:1–9. <https://doi.org/10.1016/j.plaphy.2014.03.006>.
- Cheng H, Ma X, Jia S, Li M, Mao P. Transcriptomic analysis reveals the changes of energy production and AsA-GSH cycle in oat embryos during seed ageing. *Plant Physiol Bioch*. 2020;153:40–52. <https://doi.org/10.1016/j.plaphy.2020.03.054>.
- Gutiérrez G, Cruz F, Moreno J, González-Hernández VA, Vázquez-Ramos JM. Natural and artificial seed ageing in maize: germination and DNA synthesis. *Seed Sci Res*. 1993;3:279–85. <https://doi.org/10.1017/S0960258500001896>.
- Han Z, Ku L, Zhang Z, Zhang J, Guo S, Liu H, et al. QTLs for seed vigor-related traits identified in maize seeds germinated under artificial aging conditions. *PLoS One*. 2014;9:e92535. <https://doi.org/10.1371/journal.pone.0092535>.
- Ku L, Cui X, Cheng F, Guo S, Qi J, Tian Z, et al. Genetic dissection of seed vigor under artificial ageing conditions using two joined maize recombinant inbred line populations. *Plant Breed*. 2014;133:728–37. <https://doi.org/10.1111/pbr.12221>.
- Wang B, Zhang Z, Fu Z, Liu Z, Hu Y, Tang J. Comparative QTL analysis of maize seed artificial aging between an immortalized F₂ population and its corresponding RILs. *Crop J*. 2016;4:30–9. <https://doi.org/10.1016/j.cj.2015.07.004>.
- Han Z, Bin W, Zhang J, Guo S, Zhang H, Xu L, et al. Mapping of QTLs associated with seed vigor to artificial aging using two RIL populations in maize (*Zea mays* L.). *Agric Sci*. 2018;09:397–415. <https://doi.org/10.4236/as.2018.94028>.
- Liu Y, Zhang H, Li X, Wang F, Lyle D, Sun L, et al. Quantitative trait locus mapping for seed artificial aging traits using an F_{2,3} population and a recombinant inbred line population crossed from two highly related maize inbreds. *Plant Breeding*. 2019;138:29–37. <https://doi.org/10.1111/pbr.12663>.
- Chen H, Osuna D, Colville L, Lorenzo O, Graeber K, Küster H, et al. Transcriptome-wide mapping of pea seed ageing reveals a pivotal role for genes related to oxidative stress and programmed cell death. *PLoS ONE*. 2013;8: e78471. <https://doi.org/10.1371/journal.pone.0078471>.
- Fleming MB, Patterson EL, Reeves PA, Richards CM, Gaines TA, Walters C. Exploring the fate of mRNA in aging seeds: protection, destruction, or slow decay? *J Exp Bot*. 2018;69:4309–21. <https://doi.org/10.1093/jxb/ery215>.
- Li L, Wang F, Li X, Peng Y, Zhang H, Hey S, et al. Comparative analysis of the accelerated aged seed transcriptome profiles of two maize chromosome segment substitution lines. *PLoS One*. 2019;14:e0216977. <https://doi.org/10.1371/journal.pone.0216977>.
- Wang B, Wang S, Tang Y, Jiang L, He W, Lin Q, et al. Transcriptome-wide characterization of seed aging in rice: identification of specific long-lived mRNAs for seed longevity. *Front Plant Sci*. 2022;13:857390. <https://doi.org/10.3389/fpls.2022.857390>.
- Sun M, Sun S, Mao C, Zhang H, Ou C, Jia Z, et al. Dynamic responses of antioxidant and glyoxalase systems to seed aging based on full-length transcriptome in oat (*Avena sativa* L.). *Antioxidants* (Basel). 2022;11. <https://doi.org/10.3390/antiox11020395>.
- Han Q, Chen K, Yan D, Hao G, Qi J, Wang C, et al. ZmDREB2A regulates ZmGH3.2 and ZmRAFS, shifting metabolism towards seed aging tolerance over seedling growth. *Plant J*. 2020;104:268–82. <https://doi.org/10.1111/tpj.14922>.
- Zhang Y, Li D, Dirk LMA, Downie AB, Zhao T. ZmAGA1 hydrolyzes RFOs late during the lag phase of seed germination, shifting sugar metabolism toward seed germination over seed aging tolerance. *J Agric Food Chem*. 2021;69:11606–15. <https://doi.org/10.1021/acs.jafc.1c03677>.
- Wang B, Yang R, Zhang Z, Huang S, Ji Z, Zheng W, et al. Integration of miRNA and mRNA analysis reveals the role of ribosome in to anti-artificial aging in sweetcorn. *Int J Biological Macromol*. 2023;240: 124434. <https://doi.org/10.1016/j.ijbiomac.2023.124434>.
- Du Y, Lin J, Jiang H, Zhao H, Zhang X, Wang R, Feng F. Genetic mapping for seed aging tolerance under multiple environments in sweet corn. *Agronomy*. 2025;15(1): 225. <https://doi.org/10.3390/agronomy15010225>.
- Usadel B, Nagel A, Thimm O, Redestig H, Blaessing OE, Palacios-Rojas N, et al. Extension of the visualization tool MapMan to allow statistical analysis of arrays, display of corresponding genes, and comparison with known responses. *Plant Physiol*. 2005;138:1195–204.
- Howell KA, Narsai R, Carroll A, Ivanova A, Lohse M, Usadel B, et al. Mapping metabolic and transcript temporal switches during germination in rice highlights specific transcription factors and the role of rna instability in the germination process. *Plant Physiol*. 2008;149:961–80. <https://doi.org/10.1104/pp.108.129874>.
- Farooq MA, Zhang X, Zafar MM, Ma W, Zhao J. Roles of reactive oxygen species and mitochondria in seed germination. *Front Plant Sci*. 2021;12. <https://doi.org/10.3389/fpls.2021.781734>.
- Li Y, Wang Y, Xue H, Pritchard HW, Wang X. Changes in the mitochondrial protein profile due to ROS eruption during ageing of elm (*Ulmus pumila* L.) seeds. *Plant Physiol Biochem*. 2017;114:72–87. <https://doi.org/10.1016/j.plaphy.2017.02.023>.
- Li W, He X, Chen Y, Jing Y, Shen C, Yang J, et al. A wheat transcription factor positively sets seed vigour by regulating the grain nitrate signal. *New Phytol*. 2020;225(4):1667–80. <https://doi.org/10.1111/nph.16234>.
- Zhang K, Zhang Y, Sun J, Meng J, Tao J. Deterioration of orthodox seeds during ageing: Influencing factors, physiological alterations and the role of reactive oxygen species. *Plant Physiol Biochem*. 2021;158:475–85. <https://doi.org/10.1016/j.plaphy.2020.11.031>.

32. Yang J, Su L, Li D, Luo L, Sun K, Yang M, et al. Dynamic transcriptome and metabolome analyses of two types of rice during the seed germination and young seedling growth stages. *BMC Genomics*. 2020;21. <https://doi.org/10.1186/s12864-020-07024-9>.
33. Liu C, Fukumoto T, Matsumoto T, Gena P, Frascaria D, Kaneko T, et al. Aquaporin OsPIP1;1 promotes rice salt resistance and seed germination. *Plant Physiol Bioch*. 2013;63:151–8. <https://doi.org/10.1016/j.plaphy.2012.11.018>.
34. Liu Y, He J, Yan Y, Liu A, Zhang H. Comparative transcriptomic analysis of two rice (*Oryza sativa* L.) male sterile line seed embryos under accelerated aging. *Plant Mol Biol Rep*. 2020;38(2):282–93. <https://doi.org/10.1007/s11105-020-01198-y>.
35. Singh S, Chhatwal H, Pandey A. Deciphering the complexity of terpenoid biosynthesis and its multi-level regulatory mechanism in plants. *J Plant Growth Regul*. 2024;43(10):3320–36. <https://doi.org/10.1007/s00344-024-11347-2>.
36. Chandra N, Pandey N. Influence of sulfur induced stress on oxidative status and antioxidative machinery in leaves of *Allium cepa* L. *Int Sch Res Notices*. 2014;2014(1): 568081. <https://doi.org/10.1155/2014/568081>.
37. Vitvitsky V, Mosharov E, Tritt M, Ataullakhanov F, Banerjee R. Redox regulation of homocysteine-dependent glutathione synthesis. *Redox Rep*. 2003;8(1):57–63. <https://doi.org/10.1179/135100003125001260>.
38. Zhou J, Zhang H, Huang Y, et al. Impact of sulfur deficiency and excess on the growth and development of soybean seedlings. *Int J Mol Sci*. 2024;25(20). <https://doi.org/10.3390/ijms252011253>.
39. Liu F, Zhao YP, Zhu HG, Zhu QH, Sun J. Simultaneous silencing of GhFAD2-1 and GhFATB enhances the quality of cottonseed oil with high oleic acid. *J Plant Physiol*. 2017;215:132–9. <https://doi.org/10.1016/j.jplph.2017.06.001>.
40. Cabrera-Santos D, Ordoñez-Salanueva CA, Sampayo-Maldonado S, Campos JE, Orozco-Segovia A, Flores-Ortiz CM. Chia (*Salvia hispanica* L.) seed soaking, germination, and fatty acid behavior at different temperatures. *Agriculture*. 2021;11:498. <https://doi.org/10.3390/agriculture11060498>.
41. Nambara E, Van Wees SCM. Plant hormone functions and interactions in biological systems. *Plant J*. 2021;105(2):287–9. <https://doi.org/10.1111/tpj.15151>.
42. Waadt R, Seller CA, Hsu PK, Takahashi Y, Munemasa S, Schroeder JI. Plant hormone regulation of abiotic stress responses. *Nat Rev Mol Cell Biol*. 2022;23(10):680–94. <https://doi.org/10.1038/s41580-022-00479-6>.
43. Dong X, Chen W, Wang W, Zhang H, Liu X, Luo J. Comprehensive profiling and natural variation of flavonoids in rice. *J Integr Plant Biol*. 2014;56:876–86. <https://doi.org/10.1111/jipb.12204>.
44. Cheah KS, Osborne DJ. DNA lesions occur with loss of viability in embryos of ageing rye seed. *Nature*. 1978;272:593–9. <https://doi.org/10.1038/272593a0>.
45. Sano N, Rajjou L, North HM, Debeaujon I, Marion-Poll A, Seo M. Staying alive: molecular aspects of seed longevity. *Plant Cell Physiol*. 2016;57:660–74. <https://doi.org/10.1093/pcp/pcv186>.
46. Gabay G, Faigenboim A, Dahan Y, Izhaki Y, Itkin M, Malitsky S, et al. Transcriptome analysis and metabolic profiling reveal the key role of α -linolenic acid in dormancy regulation of European pear. *J Exp Bot*. 2019;70:1017–31. <https://doi.org/10.1038/s41438-020-0287-3>.
47. Cho K, Cho KS, Sohn HB, Ha IJ, Hong SY, Lee H, et al. Network analysis of the metabolome and transcriptome reveals novel regulation of potato pigmentation. *J Exp Bot*. 2016;67:1519–33. <https://doi.org/10.1093/jxb/erv549>.
48. Li WY, Chen BX, Chen ZJ, Gao YT, Chen Z, Liu J. Reactive oxygen species generated by NADPH oxidases promote radicle protrusion and root elongation during rice seed germination. *Int J Mol Sci*. 2017;18:110. <https://doi.org/10.3390/ijms18010110>.
49. Guan YJ, Hu J, Wang ZF, Zhu SJ, Wang JC, Knapp A. Time series regression analysis between changes in kernel size and seed vigor during developmental stage of sh2 sweet corn (*Zea mays* L.) seeds. *Sci Hortic-Amsterdam*. 2013;154:25–30. <https://doi.org/10.1016/j.scienta.2013.02.016>.
50. Langdon WB. Performance of genetic programming optimised Bowtie2 on genome comparison and analytic testing (GCAT) benchmarks. *Bio-Data Min*. 2015;8(1):1. <https://doi.org/10.1186/s13040-014-0034-0>.
51. Kim D, Pertea G, Trapnell C, et al. TopHat2: accurate alignment of transcriptomes in the presence of insertions, deletions and gene fusions. *Genome Biol*. 2013;14(4):R36. <https://doi.org/10.1186/gb-2013-14-4-r36>.
52. Anders S, Pyl PT, Huber W. HTSeq—a python framework to work with high-throughput sequencing data. *Bioinformatics*. 2015;31(2):166–9. <https://doi.org/10.1093/bioinformatics/btu638>.
53. Wagner GP, Kin K, Lynch VJ. Measuring the relative contributions of transcript abundance and length to gene expression. *PLoS One*. 2012;7(10):e47740. <https://doi.org/10.1371/journal.pone.0047740>.
54. Love MI, Huber W, Anders S. Moderated estimation of fold change and dispersion for RNA-seq data with DESeq2. *Genome Biol*. 2014;15:550. <https://doi.org/10.1186/s13059-014-0550-8>.
55. Alexa A, Rahnenfuhrer J. topGO—an open source software package for gene ontology enrichment analysis. *Bioinformatics*. 2020;36(10):3076–8. <https://doi.org/10.1093/bioinformatics/btaa071>.
56. Moriya Y, Itoh M, Okuda S, et al. KAAS: an automatic genome annotation and pathway reconstruction server. *Nucleic Acids Res*. 2007;35(Web Server issue):W182–5. <https://doi.org/10.1093/nar/gkm368>.
57. Tan W, Guo X, Wang Z, Zhang R, Tang C, Jiang B, et al. Metabolic profiles and morphological characteristics of leaf tips among different sweet potato (*Ipomoea batatas* Lam.) varieties. *J Int Agri*. 2024;23:494–510. <https://doi.org/10.1016/j.jia.2023.04.029>.
58. Huang J, Cai M, Long Q, Liu L, Lin Q, Jiang L, et al. OsLOX2, a rice type I lipoxygenase, confers opposite effects on seed germination and longevity. *Transgenic Res*. 2014;23:643–55. <https://doi.org/10.1007/s11248-014-9803-2>.
59. Livak KJ, Schmittgen TD. Analysis of relative gene expression data using real-time quantitative PCR and the $2^{-\Delta\Delta CT}$ method. *Methods*. 2001;25:402–8. <https://doi.org/10.1006/meth.2001.1262>.

Publisher's Note

Springer Nature remains neutral with regard to jurisdictional claims in published maps and institutional affiliations.